ACS APPLIED POLYMER MATERIALS

pubs.acs.org/acsapm
Article

Concept of Triphenylamine Main Chains with Dual Electroactive Nitrogen Centers toward Record-High Stable Electrochromic Polyamides

Yaw-Terng Chern,* Chien-Cheng Yen, Yong-Hsien Lin, Yu-Jen Shao, Yu-Ting Kao, and Guey-Sheng Liou*

Cite This: ACS Appl. Polym. Mater. 2025, 7, 10730−10740

Read Online

ACCESS | Metrics & More | Article Recommendations | Supporting Information

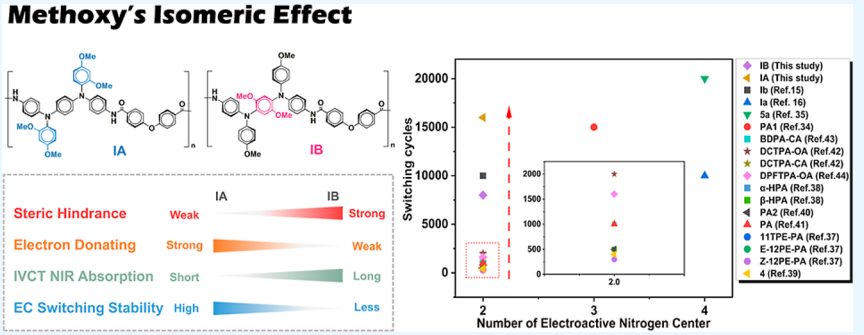

ABSTRACT: Two novel electrochromic (EC) polyamides (PAs) with dual electroactive nitrogen sites, **IA** and **IB**, were synthesized from 4,4′-dicarboxydiphenyl ether with *N*,*N*′-bis(4-aminophenyl)-*N*,*N*′-bis(2,4-dimethoxyphenyl)benzene-1,4-diamine (2) and *N*,*N*′-bis(4-aminophenyl)-*N*,*N*′-bis(4-methoxyphenyl)-2,5-dimethoxybenzene-1,4-diamine (4), respectively. **IA** demonstrated superior EC performances, including multiple color changes, intense absorption in the near-infrared (NIR) region, fast switching speed, and exceptional EC stability (after 16,000 switching cycles in the first oxidation stage, only 4.0% coloration efficiency (CE) decay at 1016 nm). The high EC stability of **IA** could originate from the resonance effect between the different redox states and the effect of electron-donating dimethoxy substituents. Although the isomeric **IA** and **IB** contain the same number of electron-donating methoxy substituents and electroactive nitrogen centers, $\mathbf{IA}^{+}$ is significantly more stable than $\mathbf{IB}^{+}$ due to the steric hindrance of the ortho-substituents (methoxy groups) at the electroactive nitrogen centers, which hinders the resonance effect of the electroactive centers for $\mathbf{IB}^{+}$. The steric hindrance for **IB** increases the oxidation potential and a broader NIR absorption. Notably, the resonance effect of the oxidized electroactive centers plays a crucial role in stabilizing cation radicals. Moreover, **IA** and **IB** exhibit strong absorption properties in the NIR and visible regions in the first oxidation state, indicating their substantial potential applications in smart windows, EC displays, and other high-performance optoelectronic devices.

KEYWORDS: *triphenylamine, electrochromism, high stability, substitution effect, mixed valence*

INTRODUCTION

Electrochromic (EC) materials are defined by their ability to undergo a reversible optical change in absorption upon electrochemically oxidized or reduced.[1,2] These materials are typically categorized into inorganic and organic chromophores. The first observation in inorganic EC materials, such as tungsten trioxide (WO_3) and Prussian blue, is widely utilized due to their excellent durability and good thermal stability.[3] However, they are limited in their ability to adjust the colors. The organic EC materials (e.g., viologens and conducting polymers) have gained considerable attention for switching among their different redox states to tune the colors. Conducting polymers offer several advantages over inorganic compounds, including outstanding CE, high optical contrast, fast switching ability, good processability, and multiple color variations.[4−10]

Among organic EC materials, π-conjugated polymers have emerged as highly versatile structures due to their adjustable donor−acceptor structures and extended electronic delocalization. For instance, carbazole-based conjugated polymers bearing substituents exhibit rapid switching (e.g., <1 s), high

Received: June 1, 2025
Revised: July 27, 2025
Accepted: July 30, 2025
Published: August 5, 2025

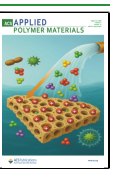

Scheme 1. Synthesis of Compounds 1 to 4

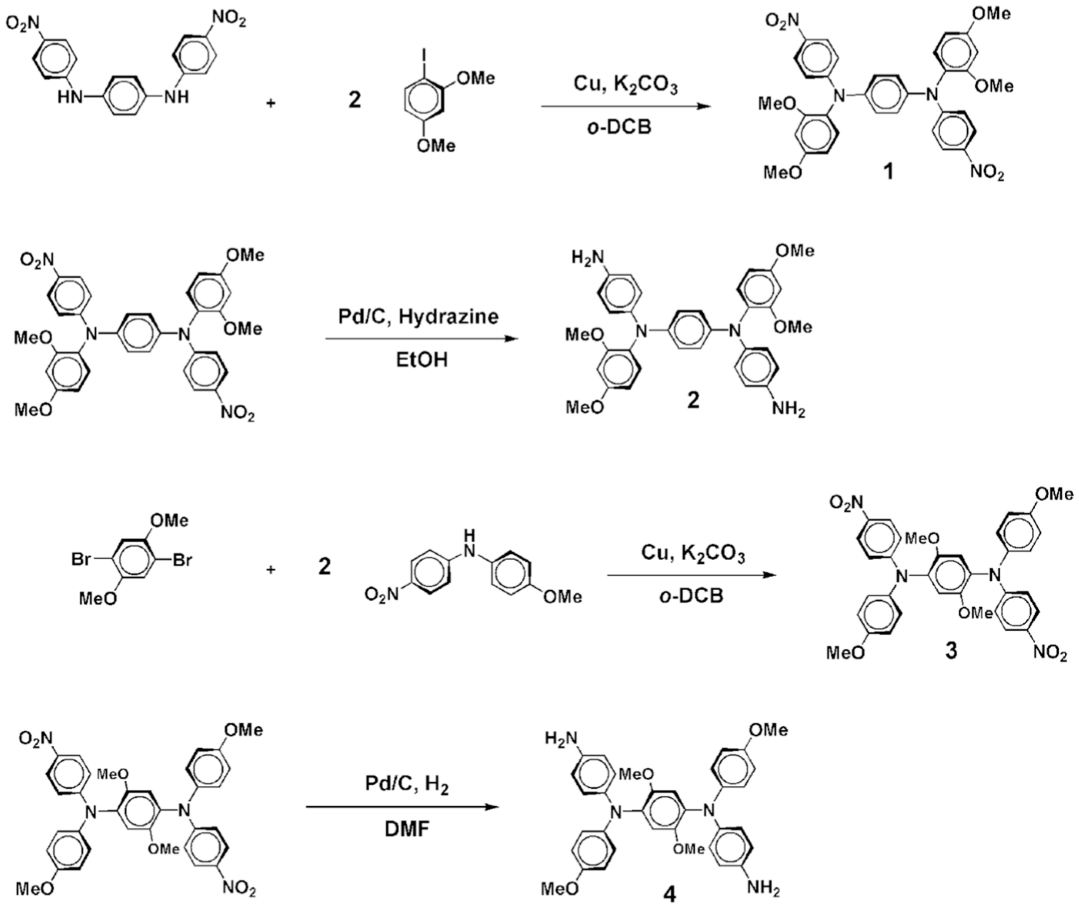

CE (>150 cm^2/C), and significant optical contrast (>40%) in the near-infrared (NIR) region.[11] Kim et al. also developed donor−acceptor structured conjugated polymers exhibiting exceptional coloration efficiencies (>200 cm^2/C), fast response times (<1 s), and excellent cycling stability, making them suitable for multifunctional smart window applications.[12] These outstanding EC performances are attributed to the effective resonance stabilization and planar backbones of the molecular structures, which facilitate efficient charge delocalization and suppress structural distortion during redox processes. These findings underscore the critical roles of resonance and steric effects in achieving long-term stability and high efficiency in electrochromic behavior.

Triphenylamine (TPA)-based polymers have attracted significant attention due to their optical transparency and colorlessness in the neutral state and intriguing EC behaviors, including high CE, quick switching responsiveness, good film-forming properties, and multiple color variations.[13−18] In recent years, when the triphenylamine (TPA) structure has only one electroactive center, its stability is usually lower. The main reason is that the free radical cations formed after oxidation lack an effective delocalization and stabilization mechanism, resulting in the inability to effectively disperse the charge, and thus, the degradation of electrochemical stability in long-term or repeated redox cycles.[13] However, dual-band electrochemical materials can effectively solve the problem of poor stability, and they have good control ability in the visible light and near-infrared spectroscopy, as well as satisfactory energy-saving efficiency, so they have attracted extensive attention.[19] These materials hold elevated potential for applications in smart windows, nonemissive displays, and adaptive camouflage.[15,20−22] For example, EC windows could mitigate the transmitted NIR radiation, potentially lowering energy consumption.[23] The mixed-valence (MV) compounds were classified by Robin and Day into three types based on the different electron coupling strengths.[24] TPA-based polymers with dual electroactive nitrogen centers have been reported as a symmetrical delocalized class II or III intervalence charge transfer (IV-CT), leading to a characteristic NIR absorption band.[25] Thus, this unique absorption could facilitate dual-band EC materials to achieve adequate energy-saving benefits.

EC materials are required to fulfill several critical criteria for practical applications, including rapid switching, substantial optical transmittance variation, high coloration efficiency (CE), and long-term stability. Among these, long-term electrochemical stability is widely recognized as one of the most challenging and essential properties for real-world implementation.[26] TPA-based polymers have attracted significant attention as mentioned previously; however, these systems often suffer from performance degradation under prolonged redox cycling. Notably, most reported TPA-containing polymers exhibit approximately a 10% CE decrement after only 2000 EC switching cycles.[14,16,27−31] To mitigate this limitation, recent studies have explored the incorporation of multiple redox-active nitrogen centers within the polymer backbone to promote charge delocalization and enhance the stability of the oxidized radical cations.[32−35] For instance, Yen and Liou developed a series of solution-

https://doi.org/10.1021/acsapm.5c01973
ACS Appl. Polym. Mater. 2025, 7, 10730−10740

processable TPA-based aromatic polyamides, in which flexible ether linkages and efficient intramolecular charge delocalization afforded high CE values (388 cm^2/C), strong near-infrared (NIR) electrochromism (λ_{max} = 1080 nm), and excellent stability over 10,000 redox cycles.[15] Similarly, star-shaped triarylamine-containing polymers designed by Liou et al. demonstrated rapid switching times (<2 s), high CE (290 cm^2/C), and minimal electrochromic degradation, underscoring the favorable impact of multibranched conjugated architectures on performance and durability.[16] Nevertheless, increasing the number of electroactive centers within TPA-containing structures typically involves complex synthetic pathways and multistep monomer design, thereby limiting the scalability and practical feasibility of such approaches. As a result, achieving high EC stability using structurally simpler systems with fewer electroactive centers remains a significant challenge. Recent findings have highlighted the importance of redox center positioning within the polymer structure. Specifically, TPA-based polymers bearing para-methoxyphenyl substituents with dual electroactive centers in the main chains exhibit markedly superior EC stability than their isomeric counterparts with similar substituents positioned in the side chains. For example, a main-chain-configured TPA polymer maintained >90% of its initial CE after 10,000 cycles, whereas a structurally related side-chain analogue showed a CE loss of 5.6% after only 1000 cycles.[15,36] These observations suggest that main-chain-oriented conjugation facilitates more effective electron delocalization and redox stabilization.

Recently, several researchers designed and synthesized TPA-based polymers with dual electroactive centers, but they still show only moderate electrochemical or EC stability.[37−44] Therefore, developing dual-electroactive centered TPA-based polymers on the main chain is worthwhile for further elevating the EC stability. Hence, this study focuses on exploring organosoluble TPA-based polyamides (PAs) with exceptional EC stability, high CE, fast switching capability, and two-stage color changes. Among the characteristics of EC performance, obtaining gratifyingly high long-term EC stability of the TPA-based polymers is relatively more challenging. Typically, cation radicals would undergo resonance on the para and ortho positions to the electroactive nitrogen center. As aforementioned, bearing a para-methoxyphenyl substituent can efficiently enhance the EC stability.[13,15] As a result, this study highlights that structural design, particularly incorporating more electron-donating methoxy groups in the ortho position, is crucial for improving the electrochemical stability of polymers. Herein, two novel EC polyamides with dual electroactive nitrogen sites, **IA** and **IB**, were prepared from 4,4′-dicarboxydiphenyl ether and two newly synthesized diamine monomers, **IA** and **IB**, containing the same number of electron-donating methoxy groups in the repeating unit, while attaching the additional two methoxy groups on different ortho positions of the electroactive diamine's pendant phenyl group or the phenyl π bridge. Furthermore, this study also elucidated the effects of the substituent position on EC performance by designing the redox-active TPA-based isomeric polyamide structures.

RESULTS AND DISCUSSION

Monomer Synthesis. Diamine monomer **2** was synthesized via two reaction steps, which start from *N*,*N*′-bis(4-nitrophenyl)benzene-1,4-diamine, as illustrated in Scheme 1. The C−N coupling reaction was carried out by reacting *N*,*N*′-bis(4-nitrophenyl)benzene-1,4-diamine with 1-iodo-2,4-dimethoxybenzene to produce intermediate **1**, which was hydrogenated to yield the new diamine monomer **2**. Similar procedures were used to prepare the new diamine monomer **4**. The C−N coupling reaction was carried out by reacting 1,4-dibromo-2,5-dimethoxybenzene with 4-methoxy-4′-nitrodiphenylamine in the presence of copper to produce intermediate **3** and then hydrogenated to prepare the new diamine **4**. The lower yield of compound **3** may be attributed to the use of a less reactive bromide (1,4-dibromo-2,5-dimethoxybenzene) in the C−N coupling reaction, instead of a more reactive iodide, and the melting point of compound **3** is higher than that of the other three compounds. We speculate that it may be related to a different configuration during crystallization than the other compounds. In addition, the relatively low yields of **2** and **4** are presumably due to the use of DMF for recrystallization. FT-IR and NMR spectroscopies were employed to characterize the chemical structures of synthesized compounds **1**−**4**. The FTIR spectra depicted in Figures S1 and S2 shows that the characteristic nitro group absorption bands of **1** and **3** were observed at approximately 1597/1591 cm^{-1} (asymmetric stretching) and 1309/1309 cm^{-1} (symmetric stretching), respectively. These nitro bands disappeared after reduction to compounds **2** and **4**, and primary amino group bands appeared at 3427/3427 cm^{-1} and 3350/3346 cm^{-1} (N−H stretching), respectively. ^1H and ^{13}C NMR spectra, as shown in Figures S5−S12, are in good agreement with the proposed molecular structures of compounds **1**−**4**. 4.72 and 4.86 ppm signals are characteristic of monomers **2** and **4** amino groups, respectively (Figures S7 and S11). The NMR and IR spectra confirmed all of the compounds reported herein. In addition, the structure of dinitro compound **3** was confirmed through single-crystal X-ray diffraction, and the single crystal was obtained via slow crystallization from DMF. As shown in Figure 1, compound **3** exhibits a propeller-shaped configuration around the TPA core, showing noncoplanar orientations, indicating that the entire structure adopts a twisted conformation.

Polymer Synthesis. According to the phosphorylation method described by Yamazaki,[45,46] two new PAs, **IA** and **IB**, were synthesized from the diamine monomer **2** and **4** with

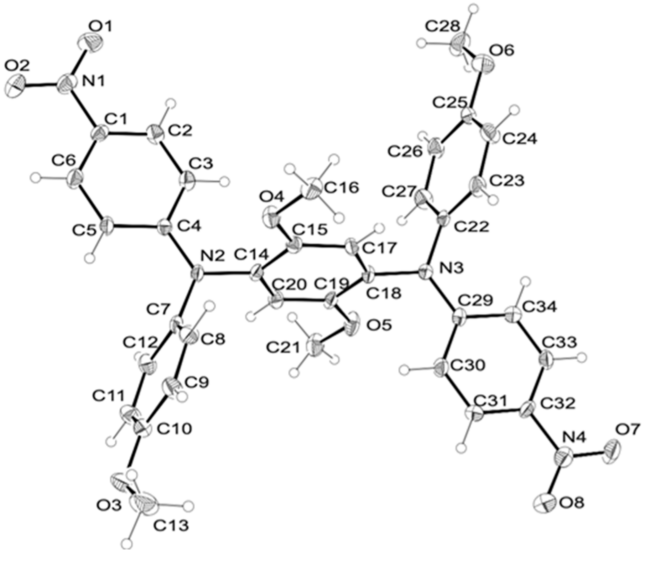

Figure 1. X-ray structure of **3**

https://doi.org/10.1021/acsapm.5c01973
ACS Appl. Polym. Mater. 2025, 7, 10730−10740

4,4′-dicarboxydiphenyl ether. The chemical structures of polyamides **IA** and **IB** are presented in Scheme 2. All

Scheme 2. Chemical Structures of Polyamides IA and IB

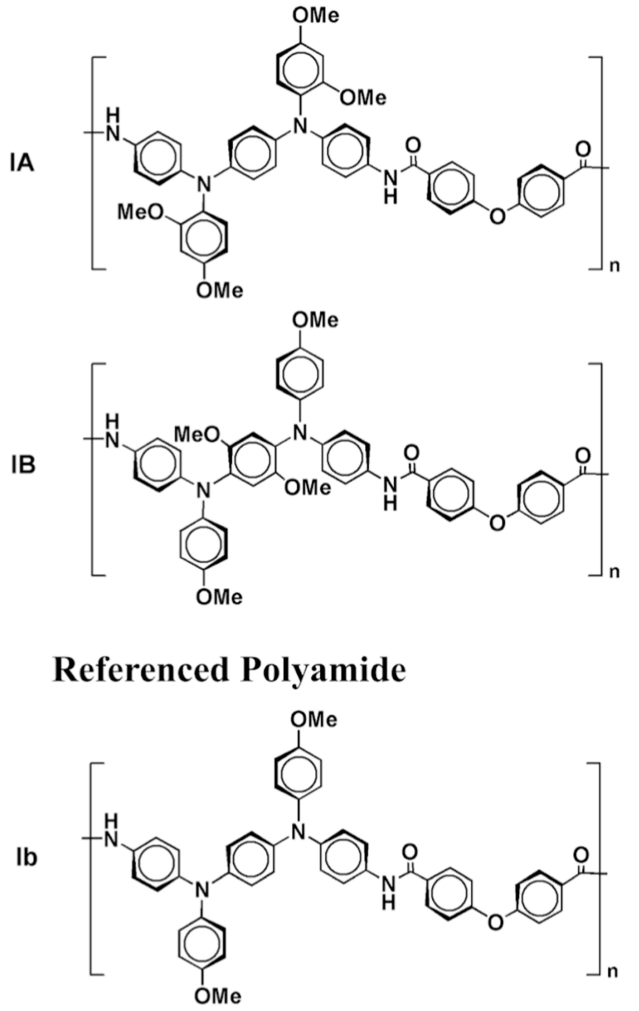

polymerization reactions proceeded homogeneously, resulting in high inherent viscosities of 0.8 and 0.5 dL/g for PAs **IA** and **IB**, respectively, as summarized in Table S1. The observed difference in inherent viscosities might be attributed to the variation in molecular rigidity and steric hindrance between the two polyamides. Specifically, the ortho-substituted structure of **IB** induces greater dihedral twisting and steric congestion, which can hinder chain growth and reduce the molecular weight, leading to a lower viscosity. In contrast, the more planar structure of **IA** facilitates better chain packing and entanglement, resulting in a higher inherent viscosity. All of the polymers were successfully prepared as transparent and tough films (Figure S15) through drop casting. IR and ^{1}H NMR spectroscopies confirmed the resulting polyamides. The IR spectra (Figures S3 and S4) exhibited characteristic amide absorption peaks at around 3316 and 3303 cm^{-1} (amide N−H stretching), as well as 1654 and 1690 cm^{-1} (amide carbonyl) for **IA** and **IB**, respectively. Furthermore, the ^{1}H NMR spectra verified the chemical structures of **IA** and **IB**, with the proton assignments detailed in Figures S13 and S14.

SOLUBILITY AND THERMAL PROPERTIES

Table S1 presents the prepared PAs' solubility in various organic solvents. **IA** and **IB** showed good solubility in the tested solvents, including DMAc, DMF, NMP, *m*-cresol, DMSO, and *o*-chlorophenol. However, **IA** shows a higher inherent viscosity (0.80 dL/g) and weight-average molecular weight (M_w = 71.5 kDa; PDI = 2.03) compared to **IB** (0.50 dL/g; 49.7 kDa; PDI = 1.87), indicating a greater degree of chain entanglement and molecular weight development. These results suggest that the more planar structure of **IA** facilitates intermolecular interactions and promotes chain growth during polymerization. Besides, when observing the chemical shifts of the amino group in ^{1}H NMR spectra, it is found that diamine **4** (4.72 ppm) exhibited a more upfield shift than diamine **2** (4.86 ppm), implying that a more basic diamine unit to undergo polymerization. Thus, the resulting polyamide **IA** would demonstrate a higher molecular weight and inherent viscosity than **IB**. The excellent solubility of these PAs makes them highly suitable for practical applications, such as inkjet printing and spin-coating, facilitating the fabrication of thin films for optoelectronic devices.

The thermal properties of the PAs were analyzed using thermogravimetric analysis (TGA) and differential scanning calorimetry (DSC), with the results summarized in Table S2. The TGA curves of both **IA** and **IB** revealed remarkable thermal stability with no obvious weight loss before 400 °C, as shown in Figure S16. The temperatures at 10% weight loss in air and nitrogen of **IA** and **IB** ranged between 405 and 434 and 403−418 °C, respectively, indicating good thermal stability. The residual wt % (char yield) of **IA** and **IB** in a nitrogen atmosphere was more than 51% at 800 °C. The glass-transition temperatures (T_g) of PAs **IA** and **IB** could be easily measured in the DSC thermograms, as shown in Figure S17. The resulting polymers exhibit relatively high T_g values, which **Ib**, **IA**, and **IB** revealed as 236, 235, and 215 °C, respectively. According to the simulation results (Figure 2), the dihedral angles of the model units were found to follow this sequence: **IA-MU** (40.47°) ∼**Ib-MU** (41.05°) < **IB-MU** (52.42°). **IB-MU** exhibits a larger torsion angle than **IA-MU** and **Ib-MU**, resulting in a more twisted backbone that hinders efficient polymer chain packing and leads to a lower glass transition temperature. In contrast, **IA**, with its smaller dihedral angle and more planar backbone, enables tighter molecular packing, thereby enhancing the thermal stability. On the other hand, the methoxy groups on the π-bridge of **IB** introduce steric hindrance that distorts the backbone conformation and disrupts $\pi-\pi$ stacking and intermolecular hydrogen bonding, compromising thermal stability. These thermal performance data further confirm the suitability of PAs **IA** and **IB** for high-temperature applications, particularly in optoelectronic devices that demand superior thermal stability and mechanical performance.

Electrochemical Properties. The cyclic voltammetry (CV) were assessed to evaluate the electrochemical properties of the polyamides deposited onto indium−tin oxide (ITO)-coated glass slides. The CV profiles for polyamides **IA** and **IB** are illustrated in Figure 3.[15] As shown in Figure 4a, the CV scans from −0.20 to 0.60 V revealed an exceptionally stable redox process over 20,000 cycles, with only a barely noticeable decrease in the peak current. Moreover, the characteristic absorption peak at 342 nm exhibits an excellent 98.2% reversibility over 20,000 cycles (Figure 4b). However, as

https://doi.org/10.1021/acsapm.5c01973
ACS Appl. Polym. Mater. 2025, 7, 10730−10740

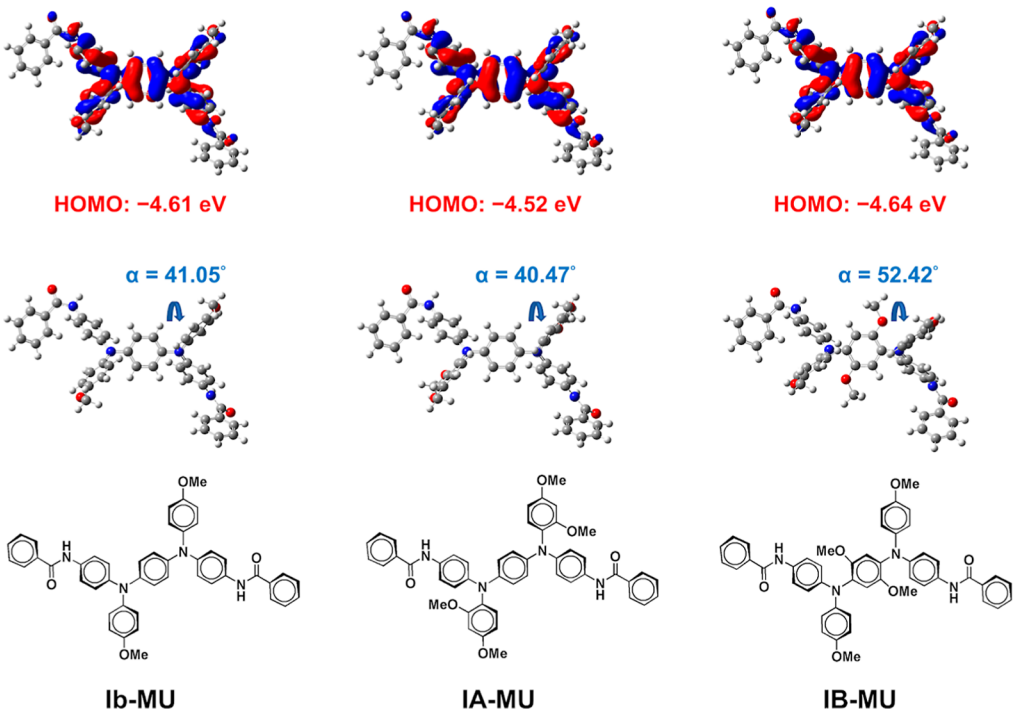

Figure 2. Calculated HOMO levels of the model units (MUs) of **Ib**, **IA**, and **IB** using DFT at the B3LYP/6−31G(d) level.

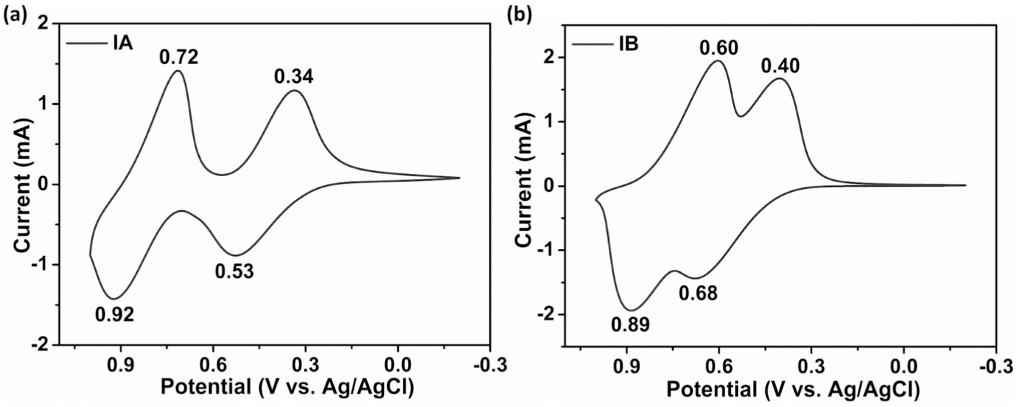

Figure 3. Cyclic voltammetric diagrams of PA films (a) **IA** (film thickness: 250 ± 30 nm) and (b) **IB** (film thickness: 250 ± 30 nm) measured on the ITO-coating (0.6 cm × 2.5 cm) glass substrate in 0.1 M TBAP/MeCN at a scan rate of 50 mV/s.

depicted in Figure 4c,d, the reversibility of **IB** could only retain 96.0% after 10,000 cycles, whereas **IA** demonstrated superior stability than **IB** at the 10,000th cycle. Therefore, **IB** did not do further testing to 20,000 cycles. This difference mainly comes from the different π-bridges in their main chains. The π bridge in **IA** consists of simple benzene rings, which provide good conjugation and planarity and help the radical cation resonate easily along the main chain, making the oxidized form more stable. In contrast, the π bridge in **IB** contains methoxy groups that twist the conformation. As a result, **IB** revealed inferior stability to **IA**.[47]

The observed redox potentials and the calculated highest occupied (HOMO) and lowest unoccupied molecular orbital (LUMO) levels of **IA** and **IB** are summarized in Table 1. The HOMO levels of **IA** and **IB**, estimated from the $E_{1/2}$ values, were −4.80 eV and −4.90 eV, respectively. Comparing homologues **IA** and **Ib** containing dual electroactive centers, we found that **IA** exhibited a lower oxidation potential than **Ib** (**IA**: E_{onset} = 0.30 V, $E_{1/2}$ = 0.44 V; **Ib**: E_{onset} = 0.42 V, $E_{1/2}$ = 0.54 V) because **IA** contains more effective electron-donating methoxy substituents in the repeating unit than does **Ib**. As a result, **IA** exhibits a higher electron density on the electroactive nitrogen of the TPA unit due to the electron-donating effect, resulting in lower E_{onset} and $E_{1/2}$. Comparing homologues **IA** and **IB**, **IB** exhibited higher oxidation potential than **IA** (**IB**: E_{onset} = 0.42 V, $E_{1/2}$ = 0.54 V; **IA**: E_{onset} = 0.30 V, $E_{1/2}$ = 0.44 V). Although **IA** and **IB** contain the same number of electron-donating methoxy substituents in the repeating unit, **IB** showed a higher oxidation potential, resulting from the relatively high steric hindrance of the ortho-substituents (methoxy groups) at the electroactive nitrogen center which affects the resonance effect between the electroactive centers. J. Reynolds et al. also reported that steric repulsion between substituents on adjacent rings increases oxidation potentials.[48,49] In addition, theoretical calculations were employed to clarify the results obtained from the electrochemical studies (Figure 2). Using the HOMO energy of **Ib-MU** (−4.61 eV) as the reference, the addition of methoxy substituents to pendant

https://doi.org/10.1021/acsapm.5c01973
ACS Appl. Polym. Mater. 2025, 7, 10730−10740

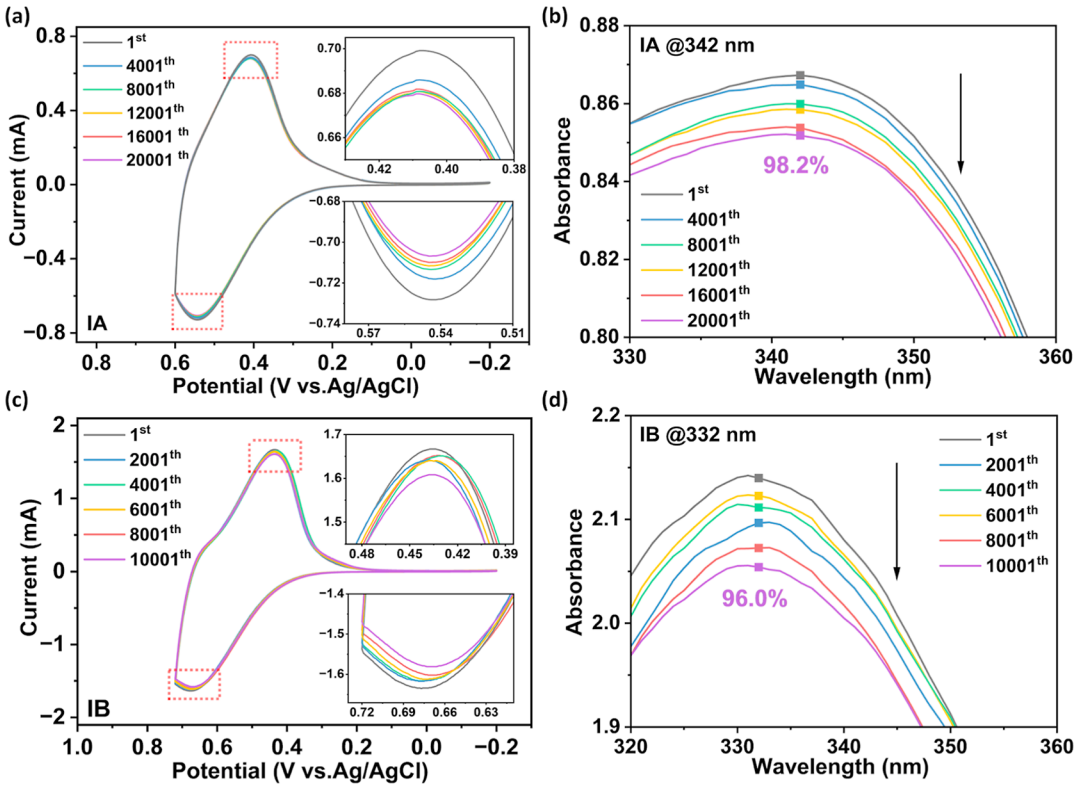

Figure 4. (a) CV stability diagram of **IA** film (thickness: 250 ± 30 nm) at the first oxidation stage (−0.20 to 0.60 V) for 20,000 cycles. (b) UV−vis spectra of **IA** film in the neutral state after different scanning cycles. (c) CV stability diagram of **IB** film (thickness: 250 ± 30 nm) at the first oxidation stage (−0.20 to 0.72 V) for 10,000 cycles. (d) UV−vis spectra of **IB** film in the neutral state after different scanning cycles.

Table 1. Electrochemical and Optical Properties of Resulting PAs

	film (nm)			oxidation potential (V)				
				$E_{1/2}$[c]				
code	λ_{max}[a]	λ_{onset}[a]	E_g (eV)[b]	E_{onset}	1st	2nd	HOMO (eV)[d]	LUMO (eV)[e]
IA	342	405	3.06	0.30	0.44	0.82	−4.80	−1.84
IB	332	402	3.08	0.42	0.54	0.75	−4.90	−1.82
Ib[f]	342	411	3.02	0.42	0.54	0.90	−4.86	−1.84

[a]UV/vis absorption measurements are in the film state. [b]Calculated in the film state by the equation: $E_g = 1240/\lambda_{onset}$, where E_g is the energy gap between HOMO and LUMO. [c]Versus Ag/AgCl in MeCN in the cyclic voltammetry. $E_{1/2}$: Average potential of the redox couple peaks. [d]Calculated from cyclic voltammetry using ferrocene/ferrocenium as reference (−4.80 eV and $E_{1/2}$ = 0.44 V). [e]LUMO = HOMO + E_g. [f]Data were cited from ref 15.

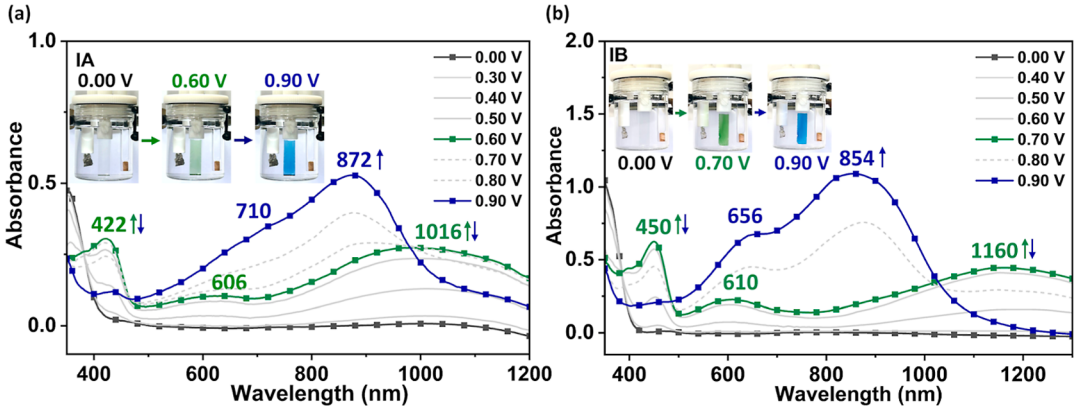

Figure 5. Absorption profiles and electrochromic behaviors of PAs (a) **IA** (film thickness: 250 ± 30 nm) and (b) **IB** (film thickness: 250 ± 30 nm) measured on ITO-coating (0.6 cm × 2.5 cm) glass substrate in 0.1 M TBAP/MeCN.

https://doi.org/10.1021/acsapm.5c01973
ACS Appl. Polym. Mater. 2025, 7, 10730−10740

Table 2. EC Switching Stability of PA IA at 0.6 V in Different Cycles

cycles[a]	ΔOD_{1016}[b]	ΔT (%)[c]	Q (mC/cm^2)[d]	η (cm^2/C)[e]	decay (%)[f]
1	0.26	45.5	1.60	162.5	0.0
2000	0.26	45.1	1.60	162.5	0.0
4000	0.25	43.7	1.54	162.3	0.0
6000	0.25	43.7	1.54	162.3	0.0
8000	0.25	43.2	1.54	162.3	0.0
10,000	0.24	42.5	1.49	161.1	1.0
12,000	0.23	41.8	1.45	158.6	2.0
14,000	0.23	41.3	1.45	158.6	2.0
16,000	0.22	40.3	1.41	156.0	4.0

[a]Times of cyclic scan by applying potential step: 0.0 V 21C6 0.6 V (V vs Ag/AgCl). [b]Optical density change at 1016 nm. [c]Optical transmittance change at 1016 nm. [d]Ejected charge is determined from in situ experiments. [e]Coloration efficiency is derived from the equation $\eta = \Delta OD/Q$. [f]Decay of coloration efficiency after cyclic scans.

anisole group (**IA-MU**) resulted in a significant increase in the HOMO energy to −4.52 eV, attributed to the electron-donating effect. Conversely, adding methoxy substituents to the π-bridge (**IB-MU**) caused the HOMO energy to decrease to −4.64 eV, which aligns with the trends observed in the aforementioned electrochemical results. To clarify this phenomenon, we observed the corresponding dihedral angles of the model units, and these results indicated that the higher oxidation potential of **IB-MU** was attributed to the ortho-substituents' steric hindrance, which weakens the electron-donating ability of each nitrogen center.

Spectroelectrochemical Behaviors. The spectroelectrochemical spectra of **IA** are presented in Figure 5a. The resulting film appeared transparent and colorless in the neutral form (0 V). When the applied voltage increased from 0 to 0.6 V, a new absorption peak emerged at 422 nm, along with a broad absorption band around 1016 nm in the near-infrared (NIR) region, and the film color changed from colorless to grass green. These spectral changes in the visible range were attributed to the formation of a stable monocation radical at the TPA center of the *N*,*N*,*N*′,*N*′-tetraphenyl-*p*-phenylenediamine (TPPA) moiety.[50] The broad NIR absorption band corresponds to intervalence charge transfer (IV-CT) excitation, involving electron transfer from the active neutral nitrogen atom to the cation radical nitrogen center in the TPPA moiety.[25] As the applied potential further increased to 0.9 V, the absorption bands corresponding to the monocation radical began to diminish, and a new broad absorption band appeared at 872 nm, accompanied by a color change from grass green to sky blue (Figure S18a). The disappearance of the previous NIR band is attributed to the further oxidation of the monocation radical species, resulting in the formation of dications in the TPPA segments. The UV−vis−NIR absorption changes observed in the **IA** film at various applied potentials were fully reversible and were accompanied by distinct color transitions. The spectroelectrochemical spectra of **IB** are presented in Figure 5b, which displayed spectroelectrochemical spectra and color changes similar to those of (Figure S18b) as **IA** because of the isomeric electroactive chemical structures. However, **IB** revealed a significantly longer λ_{max} of nearly 150 nm shift and a broader NIR absorption at the first oxidation stage compared to **IA**. Red-shifted absorption wavelength in the NIR region is ascribed to a weaker electronic coupling between two redox-active centers that could be attributed to the steric hindrance of the ortho-substituents (methoxy groups) on the π bridge, hindering the resonance ability of the electroactive centers for **IB**$^+$.

IA and **IB** exhibit notable optical contrast in the visible and NIR regions. The transmittance change (ΔT (%)) for **IA** reached 44.7% at 1016 nm and 70.2% at 872 nm in the first and second oxidation states, respectively. Similarly, **IB** showed a ΔT of 68.3% at 1160 nm and 91.5% at 854 nm during the first and second oxidation stages, respectively. These exceptional absorbance properties in both the visible and NIR regions highlighted the significant potential of **IA** and **IB** for dual-band electrochromic applications.

Electrochromic Switching Behaviors. The EC switching stability and response times of the polyamides were assessed by monitoring the absorption changes during potential step applications in kinetic studies. The switching data for the PAs **IA** and **IB** are presented in Figure S19. The electrochromic CE ($\eta = \Delta OD/Q$) and injected charge after different controlled switching cycles were monitored and are summarized in Tables 2, 3, S4, and S5. The results for ΔT, CE, and the percentage of CE decay are illustrated in Figure 6. The gradual decline in electrochromic performance during repeated switching cycles could be attributed to several factors. First, repeated oxidation and reduction of the resulting polymers may lead to irreversible side reactions of radical species, such as degradation or coupling, resulting in fewer active redox centers. Second, repeated structural reorganization of the polymer backbone could cause conformational fatigue, which impairs charge delocalization and transfer efficiency. In

Table 3. EC Switching Stability of PA IB at 0.6 V in Different Cycles

cycles[a]	ΔOD_{1160}[b]	ΔT (%)[c]	Q (mC/cm^2)[d]	η (cm^2/C)[e]	decay (%)[f]
1	0.38	58.4	0.68	560	0.0
1000	0.33	53.3	0.65	509	9.1
2000	0.32	52.1	0.65	492	12.1
3000	0.31	51.5	0.64	490	12.5
4000	0.30	49.9	0.64	469	16.3
5000	0.29	49.1	0.63	465	17.0
6000	0.27	46.4	0.60	452	19.3
7000	0.27	46.3	0.60	450	19.6
8000	0.26	45.2	0.59	442	21.1

[a]Times of cyclic scan by applying potential step: 0.0 V ⇆ 0.6 V (V vs Ag/AgCl). [b]Optical density change at 1160 nm. [c]Optical transmittance change at 1160 nm. [d]Ejected charge is determined from in situ experiments. [e]Coloration efficiency is derived from the equation $\eta = \Delta OD/Q$. [f]Decay of coloration efficiency after cyclic scans.

https://doi.org/10.1021/acsapm.5c01973
ACS Appl. Polym. Mater. 2025, 7, 10730−10740

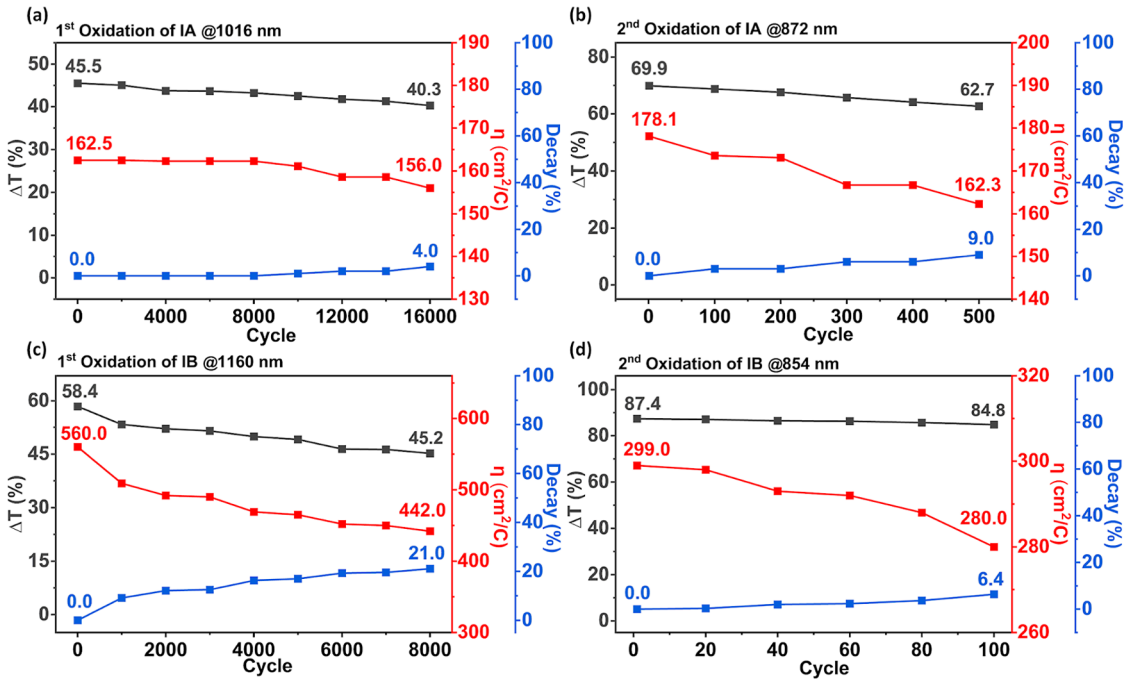

Figure 6. Potential step absorptiometry and current consumption of PAs. Plots of ΔT, CE, and the decay percentage of **IA** for (a) the first oxidation state at 1016 and (b) the second oxidation state at 872. (c) Plots of ΔT, CE, and the decay percentage of **IB** for the first oxidation state at 1160 and (d) the second oxidation state at 854, and all the results were measured in MeCN with 0.1 M TBAP as the supporting electrolyte.

addition, electrolyte infiltration or interfacial instability may weaken the charge injection and redox activity. These combined effects decrease ΔT, lead to longer response times, and reduce the CE.

During the first EC switching test (between 0.0 and 0.6 V), **IA** showed outstanding switching stability with gratifying reversibility of only 4.0% decay of the CE (156.0−162.5 cm^2/C) at 1016 nm over continuous 16,000 cycles (Figure 6a). This exceptional stability could be attributed to the stable electrochemical properties upon the redox process of **IA** and also the strong adhesion between the polymer film and the ITO substrate. For the further oxidation switching between 0.0 and 0.9 V, **IA** revealed relatively poorer switching stability and reversibility than those in the first oxidation state, with 9.0% decay of the CE (162.3−178.1 cm^2/C) at 872 nm over continuous 500 cycles (Figure 6b). For **IB**, switching stability and reversibility of the first oxidation stage between 0 and 0.6 V exhibited 21.1% decay of the CE (560.0−442.0 cm^2/C) at 1160 nm over continuous 8000 cycles (Figure 6c). **IB** exhibited relatively inferior switching stability and reversibility for further oxidation switching between 0.0 and 0.9 V, with a 6.4% decay of CE (280.0−299.0 cm^2/C) at 854 nm over continuous 100 cycles (Figure 6d).

IA demonstrated excellent stability at 1016 and 872 nm in the first and second EC processes, respectively, as summarized in Tables 2 and S4. Furthermore, the response times for **IA**, calculated at 90% of the full ΔT, demonstrated 3.9/1.1 s (coloring/bleaching) at 1016 nm and 5.0/0.9 s at 872 nm for the first and second EC stages, respectively. **IB** demonstrated a 4.3/0.9 s response time at 1160 nm and 3.4/2.5 s at 854 nm for the first and second EC stages. In summary, PAs **IA** and **IB** switched rapidly at the first and second stages.

Steric and Resonance Effects on Electrochromic Durability. The EC stability of the redox-active polyamides for long-term switching between the oxidized and neutral states is essential for practical application. Two key factors influence the radical stability: first, the electron-donating or -withdrawing ability of substituents; second, the resonance effect of electron delocalization across the electroactive nitrogen centers, both of which significantly impact EC stability. The electrochemical stability between structure-related polyamides of **IA**, **IB**, and the corresponding **Ib** was compared and is summarized in Table 4.

Table 4. Long-Term Stability of the Prepared PAs

polyamide	potential (V)	η (cm^2/C)[a]	cycles[b]	ΔT (%)[c]	decay (%)[d]
IA	0.0 ↔ 0.6	163	16,000	45.5	4.0
IB	0.0 ↔ 0.6	560	8000	58.4	21.1
Ib[e]	0.0 ↔ 0.7	388	10,000	54.0	4.89

[a]Initial coloration efficiency. [b]Times of the cyclic scan by applying a potential step. [c]Initial contrast of the optical transmittance change at 1016 nm for **IA**, 1160 nm for **IB**, and 433 nm for **Ib**. [d]Decay of the coloration efficiency after cyclic scans. [e]The data were cited from the **Ib** in ref 15.

The trend of the electrochemical stability in the first oxidation stage is $\mathbf{IA}^+ > \mathbf{Ib}^+ > \mathbf{IB}^+$. **IA** exhibits an EC stability significantly higher than that of **Ib** in the first oxidation stage. Since cation radicals are considered to be electron-deficient, stabilizing cation radicals from the electron-donating methoxy group could be expected. Consequently, the higher EC stability of **IA** could be ascribed to the more electron-donating methoxy substituents in the repeating unit than **Ib**, resulting in superior EC stability. Intriguingly, **Ib** exhibits EC stability significantly higher than that of **IB** in the first oxidation stage, even though **IB** contains more electron-donating methoxy substituents in the repeating unit than **Ib** and with the same number of electroactive nitrogen centers and could be expected to form a more stable $\mathbf{IB}^+$. However, $\mathbf{IB}^+$ has lower stability than $\mathbf{Ib}^+$,

https://doi.org/10.1021/acsapm.5c01973
ACS Appl. Polym. Mater. 2025, 7, 10730−10740

which might be caused by the relatively high steric hindrance of the ortho-substituents (methoxy groups) at the electroactive nitrogen centers, hindering the electron delocalization between the two electroactive centers.[47] These results suggest that the resonance ability of the electroactive nitrogen center is far more imperative than that of the electron-donating group to stabilize cation radicals. Furthermore, although **IA** and **IB** contain the same number of electron-donating methoxy substituents, $\mathbf{IA}^{+}$ displayed significantly higher stability than $\mathbf{IB}^{+}$, also attributed to the relatively high steric hindrance of the ortho-substituents (methoxy groups). Notably, the resonance effect of the electroactive centers plays a key role in stabilizing the cation radicals.

The long-term switching stability of polymers is crucial for practical applications. Figure 7 and Table S6 illustrate the relationship between the number of electroactive nitrogen centers and the electrochromic stability in the first oxidation stage. In general, polymers with a higher number of electroactive nitrogen centers exhibit better electrochromic stability. Notably, polymer **IA** investigated in this study, despite containing only two electroactive centers, demonstrated exceptional electrochromic stability, with only a 2% decrease in coloration efficiency after 12,000 switching cycles. This result highlights the excellent stability of **IA** and emphasizes its synthetic advantage by avoiding the structural complexity often associated with the incorporation of multiple electroactive nitrogen centers.

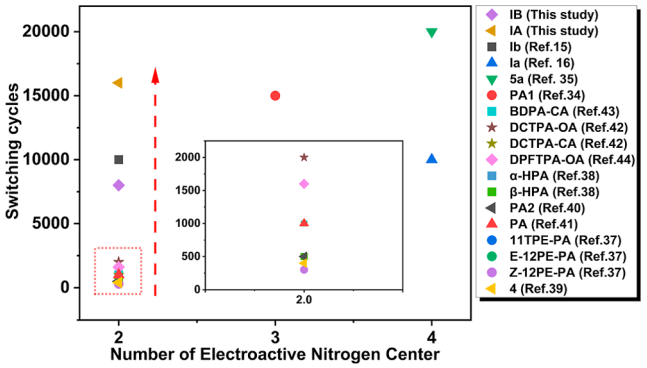

Figure 7. Percentage decay of coloration efficiency (CE) of triarylamine-based polymers after repeated switching cycles at the first oxidation potential.

CONCLUSION

Two novel electrochromic polyamides, **IA** and **IB**, bearing dual electroactive nitrogen centers and methoxy-substituted triphenylamine (TPA) units, were successfully synthesized from 4,4′-dicarboxydiphenyl ether and newly designed diamine monomers. This isomeric structural difference results in distinct electrochromic (EC) properties. Polyamide **IA** exhibited superior EC performance, including a rapid switching time (3.9/1.1 s at 1016 nm) and exceptional long-term stability with only 4.0% CE decay after 16,000 cycles. However, it has a smaller transmittance contrast (ΔT = 45.5% at 1016 nm) and coloration efficiency value. In contrast, **IB** with the methoxy-substituted groups on the π bridge reveals higher absorptivity in the visible and NIR region, higher transmittance contrast (ΔT = 58.4% at 1160 nm), and remarkable coloration efficiency up to 560 cm^2/C. This finding indicates that the methoxy substitution on the π bridge could demonstrate stronger auxochrome ability. Nevertheless, **IB** showed slower switching, a broader and red-shifted NIR absorption, and a higher CE decay of 21.1% after 8000 cycles, likely due to steric hindrance and a large dihedral angle (~52°) that disrupted π-conjugation and hindered effective resonance stabilization of the cation radicals.

Notably, when compared to a previously reported reference polyamide with similar TPA-based backbones, **IA** demonstrated comparable or even superior EC stability, despite having a simpler structure with only two electroactive nitrogen centers. Although structurally more complex, the reference polymer exhibited a similar first-stage absorption profile and dual-stage redox behavior but required more extensive conjugation or additional electroactive units to achieve long-term stability. These results underscore the effectiveness of substituent positional control as a rational molecular design strategy to enhance EC performance without increasing synthetic complexity. Overall, this study reveals a new structure−property relationship that advances the development of durable and high-efficiency EC polymers.

ASSOCIATED CONTENT

Supporting Information

The Supporting Information is available free of charge at https://pubs.acs.org/doi/10.1021/acsapm.5c01973.

Experimental section, FT-IR spectra, ^{1}H and ^{13}C NMR, TMA, DMA, inherent viscosity and solubility properties, electrochemical properties, and single-crystal information (PDF)

Crystallographic data for **3** (CCDC 2448143) (CIF)

AUTHOR INFORMATION

Corresponding Authors

Yaw-Terng Chern − *Department of Chemical Engineering, National Taiwan University of Science and Technology, Taipei 106335, Taiwan*; Email: ytchern@mail.ntust.edu.tw

Guey-Sheng Liou − *Institute of Polymer Science and Engineering, National Taiwan University, Taipei 106335, Taiwan*; orcid.org/0000-0003-3725-3768; Email: gsliou@ntu.edu.tw

Authors

Chien-Cheng Yen − *Department of Chemical Engineering, National Taiwan University of Science and Technology, Taipei 106335, Taiwan*

Yong-Hsien Lin − *Department of Chemical Engineering, National Taiwan University of Science and Technology, Taipei 106335, Taiwan*

Yu-Jen Shao − *Institute of Polymer Science and Engineering, National Taiwan University, Taipei 106335, Taiwan*; orcid.org/0009-0003-6302-7761

Yu-Ting Kao − *Institute of Polymer Science and Engineering, National Taiwan University, Taipei 106335, Taiwan*

Complete contact information is available at: https://pubs.acs.org/10.1021/acsapm.5c01973

Author Contributions

Yaw-Terng Chern conceived the idea, designed the experiments, and wrote the manuscript with help and feedback from all authors. Chien-Cheng Yen: data curation and investigation. Yong-Hsien Lin: data curation and investigation. Guey-Sheng Liou: methodology, designed the experiments, and revised the

https://doi.org/10.1021/acsapm.5c01973
ACS Appl. Polym. Mater. 2025, 7, 10730−10740

manuscript. Yu-Jen Shao revised and organized the manuscript Yu-Ting Kao conducted the experiments and analyzed the results.

Notes

The authors declare no competing financial interest.

■ ACKNOWLEDGMENTS

We appreciate the financial support provided by the National Science and Technology Council of Taiwan (111-2628-E-011-008-MY3).

■ REFERENCES

(1) Rosseinsky, D. R.; Mortimer, R. J. Electrochromic systems and the prospects for devices. *Adv. Mater.* **2001**, *13* (11), 783−793.
(2) Monk, P.; Mortimer, R.; Rosseinsky, D. *Electrochromism and Electrochromic Devices*; CUP, 2007.
(3) Dautremont-Smith, W. Transition metal oxide electrochromic materials and displays: a review: Part 1: oxides with cathodic coloration. *Displays* **1982**, *3* (1), 3−22.
(4) Skotheim, T. A. *Handbook of Conducting Polymers*; CRC Press, 1997.
(5) Kumar, A.; Welsh, D. M.; Morvant, M. C.; Piroux, F.; Abboud, K. A.; Reynolds, J. R. Conducting poly (3, 4-alkylenedioxythiophene) derivatives as fast electrochromics with high-contrast ratios. *Chem. Mater.* **1998**, *10* (3), 896−902.
(6) Schwendeman, I.; Hickman, R.; Sönmez, G.; Schottland, P.; Zong, K.; Welsh, D. M.; Reynolds, J. R. Enhanced contrast dual polymer electrochromic devices. *Chem. mater.* **2002**, *14* (7), 3118−3122.
(7) Neo, W. T.; Ye, Q.; Chua, S.-J.; Xu, J. Conjugated polymer-based electrochromics: materials, device fabrication and application prospects. *J. Mater. Chem. C* **2016**, *4* (31), 7364−7376.
(8) Huang, Z.-J.; Li, F.; Xie, J.-P.; Mou, H.-R.; Gong, C.-B.; Tang, Q. Electrochromic materials based on tetra-substituted viologen analogues with broad absorption and good cycling stability. *Sol. Energy Mater. Sol. Cells* **2021**, *223*, 110968.
(9) Feng, F.; Guo, S.; Ma, D.; Wang, J. An overview of electrochromic devices with electrolytes containing viologens. *Sol. Energy Mater. Sol. Cells* **2023**, *254*, 112270.
(10) Liu, Y.; Xing, Z.; Jia, S.; Shi, X.; Chen, Z.; Jiang, Z. Research progress in special engineering plastic-based electrochromic polymers. *Materials* **2024**, *17* (1), 73.
(11) Bezgin Carbas, B. Disruptive Electrochromic Materials: Carbazole-Based Conjugated Polymers. *ACS Appl. Polym. Mater.* **2025**, *7* (7), 4051−4076.
(12) Kim, J.; Rémond, M.; Kim, D.; Jang, H.; Kim, E. Electrochromic conjugated polymers for multifunctional smart windows with integrative functionalities. *Adv. Mater. Technol.* **2020**, *5* (6), 1900890.
(13) Chang, C.-W.; Liou, G.-S.; Hsiao, S.-H. Highly stable anodic green electrochromic aromatic polyamides: synthesis and electrochromic properties. *J. Mater. Chem.* **2007**, *17* (10), 1007−1015.
(14) Liou, G.-S.; Lin, H.-Y. Synthesis and electrochemical properties of novel aromatic poly (amine−amide) s with anodically highly stable yellow and blue electrochromic behaviors. *Macromolecules* **2009**, *42* (1), 125−134.
(15) Yen, H.-J.; Liou, G.-S. Solution-processable novel near-infrared electrochromic aromatic polyamides based on electroactive tetraphenyl-p-phenylenediamine moieties. *Chem. Mater.* **2009**, *21* (17), 4062−4070.
(16) Yen, H.-J.; Lin, H.-Y.; Liou, G.-S. Novel starburst triarylamine-containing electroactive aramids with highly stable electrochromism in near-infrared and visible light regions. *Chem. Mater.* **2011**, *23* (7), 1874−1882.
(17) Sun, N.; Su, K.; Zhou, Z.; Tian, X.; Jianhua, Z.; Chao, D.; Wang, D.; Lissel, F.; Zhao, X.; Chen, C. High-performance emission/color dual-switchable polymer-bearing pendant tetraphenylethylene (TPE) and triphenylamine (TPA) moieties. *Macromolecules* **2019**, *52* (14), 5131−5139.
(18) Zhang, W.-j.; Lin, X.-c.; Li, F.; Huang, Z.-j.; Gong, C.-b.; Tang, Q. Multicolored electrochromic and electrofluorochromic materials containing triphenylamine and benzoates. *New J. Chem.* **2020**, *44* (38), 16412−16420.
(19) Yuan, C.; Kuang, G.; Yin, H.; Zeb, A.; Yin, P.; Zhang, C.; Tao, Y.; Guo, Y.; Zhang, S. "Dark-to-Warm" Smart Windows Enabled by Black-to-Black Electrochromic Copolymers with Minimal Visible and Remarkable NIR Modulation. *Macromolecules* **2024**, *57* (13), 6100−6108.
(20) Brooke, R.; Mitraka, E.; Sardar, S.; Sandberg, M.; Sawatdee, A.; Berggren, M.; Crispin, X.; Jonsson, M. P. Infrared electrochromic conducting polymer devices. *J. Mater. Chem. C* **2017**, *5* (23), 5824−5830.
(21) Hao, Q.; Li, Z.-J.; Lu, C.; Sun, B.; Zhong, Y.-W.; Wan, L.-J.; Wang, D. Oriented two-dimensional covalent organic framework films for near-infrared electrochromic application. *J. Am. Chem. Soc.* **2019**, *141* (50), 19831−19838.
(22) Zeng, J.; Wang, Y.; Rajan, K.; Xiao, Z.; Rehman Sagar, R. U.; Liu, P. Transparent-to-black electrochromic smart windows based on *N*,*N*,*N*′,*N*′-Tetraphenylbenzidine derivatives and tungsten trioxide with high adjustment ability for visible and near-infrared light. *Sol. Energy Mater. Sol. Cells* **2021**, *226*, 111070.
(23) Niu, J.; Wang, Y.; Zou, X.; Tan, Y.; Jia, C.; Weng, X.; Deng, L. Infrared electrochromic materials, devices and applications. *Appl. Mater. Today* **2021**, *24*, 101073.
(24) Robin, M. B.; Day, P. Mixed valence chemistry-a survey and classification. In *Advances in inorganic chemistry and radiochemistry*; Academic Press, 1968; Vol. *10*, pp 247−422.
(25) Lambert, C.; Nöll, G. The class II/III transition in triarylamine redox systems. *J. Am. Chem. Soc.* **1999**, *121* (37), 8434−8442.
(26) Sonmez, G.; Meng, H.; Wudl, F. Organic polymeric electrochromic devices: polychromism with very high coloration efficiency. *Chem. mater.* **2004**, *16* (4), 574−580.
(27) Chang, C.-W.; Chung, C.-H.; Liou, G.-S. Novel anodic polyelectrochromic aromatic polyamides containing pendent dimethyltriphenylamine moieties. *Macromolecules* **2008**, *41* (22), 8441−8451.
(28) Hou, Y.; Kong, L.; Ju, X.; Liu, X.; Zhao, J.; Niu, Q. Multichromic polymers containing alternating bi (3-methoxythiophene) and triphenylamine based units with para-protective substituents. *Materials* **2016**, *9* (9), 779.
(29) Hsiao, S.-H.; Wu, C.-N. Electrochemical and electrochromic studies of redox-active aromatic polyamides with 3, 5-dimethyltriphenylamine units. *J. ELECTROANAL CHEM* **2016**, *776*, 139−147.
(30) Wu, T.-Y.; Chung, H.-H. Applications of tris(4-(thiophen-2-yl)phenyl)amine- and dithienylpyrrole-based conjugated copolymers in high-contrast electrochromic devices. *Polymers* **2016**, *8* (6), 206.
(31) Cai, S.; Wang, S.; Wei, D.; Niu, H.; Wang, W.; Bai, X. Multifunctional polyamides containing pyrrole unit with different triarylamine units owning electrochromic, electrofluorochromic and photoelectron conversion properties. *J. Electroanal Chem* **2018**, *812*, 132−142.
(32) Chern, Y.-T.; Lin, Y.-Q.; Han, J.-R.; Chiu, Y.-C. Achieving ultrahigh electrochromic stability of triarylamine-based polymers by the design of five electroactive nitrogen centers. *Mater. Today Chem.* **2024**, *40*, 102236.
(33) Chern, Y.-T.; Yen, C.-C.; Wang, J.-M.; Lu, I.-S.; Huang, B.-W.; Hsiao, S.-H. Redox-Stable and Multicolor Electrochromic Polyamides with Four Triarylamine Cores in the Repeating Unit. *Polymers* **2024**, *16* (12), 1644.
(34) Chern, Y.-T.; Zhang, S.-J.; Ho, S.-J.; Shao, Y.-J.; Wang, Y.-J.; Liou, G.-S. Substituents and Resonance Effects on the Electrochemical Stability of Polyelectrochromic Triarylamine-Based Polymers. *ACS Appl. Polym. Mater.* **2024**, *6* (9), 5256−5267.
(35) Chern, Y.-T.; Zhang, Z.-Y.; Wang, J.-J.; Lin, P.-L.; Chiu, Y.-C.; Wang, Y.-J.; Lin, C.-H.; Liou, G.-S. Concept of triphenylamine side chains with four electroactive nitrogen centers toward record-high

https://doi.org/10.1021/acsapm.5c01973
ACS Appl. Polym. Mater. 2025, 7, 10730−10740

stable electrochromic polyamides. *J. Mater. Chem. C* **2024**, *12* (24), 8804−8812.
(36) Liou, G.-S.; Chang, C.-W. Highly stable anodic electrochromic aromatic polyamides containing *N,N,N′,N′*-tetraphenyl-*p*-phenylenediamine moieties: synthesis, electrochemical, and electrochromic properties. *Macromolecules* **2008**, *41* (5), 1667−1674.
(37) Sun, N.; Su, K.; Zhou, Z.; Wang, D.; Fery, A.; Lissel, F.; Zhao, X.; Chen, C. "Colorless-to-black" electrochromic and AIE-active polyamides: an effective strategy for the highest-contrast electrofluorochromism. *Macromolecules* **2020**, *53* (22), 10117−10127.
(38) Su, K.; Sun, N.; Tian, X.; Li, X.; Chao, D.; Wang, D.; Zhou, H.; Chen, C. Novel polyamides with pendant p-phenylenediamine and *α*-/*β*-substituted naphthalene: Synthesis, characteristics, and effects of substitution sites on electro-switchable optical behaviors. *Mater. Today Chem.* **2021**, *22*, 100536.
(39) Li, X.; Su, K.; Zeng, Q.; Wang, D.; Zhao, X.; Chen, C. Highly stable electrochromism and electrofluorochromism derived from a bifunctional polyamide containing conjugated bis (diphenylamine-spirodifluorene) moieties. *Dyes Pigm.* **2022**, *199*, 110072.
(40) Rusu, R.-D.; Damaceanu, M.-D.; Ursache, S.; Constantin, C.-P. Tuning the main electrochromic features by polymer backbone variation of triphenylamine-based polyamides. *J. Photochem. Photobiol.* **2023**, *435*, 114272.
(41) Constantin, C.-P.; Balan-Porcarasu, M.; Lisa, G. Exploring innovative synthetic solutions for advanced polymer-based electrochromic energy storage devices: Phenoxazine as a promising chromophore. *J. Energy Chem.* **2024**, *91*, 433−452.
(42) An, J.; Cai, W.; Zheng, W.; Zheng, Z.; Ming, X.; Niu, H.; Wang, W. High-contrast electrochromic nano fiber films changing from yellow-green to black based on butterfly monomer for smart windows and self-adaptive camouflage. *J. Colloid Interface Sci.* **2025**, *693*, 137559.
(43) Li, D.; Xu, Y.; Dai, J.; Qin, Q.; Fu, H.; Wang, X.; Xu, Y.; Zeng, B.; Luo, W.; Dai, L. Solution processable triarylamine-based polyamide for electrochromic supercapacitors and smart displays with energy reuse. *J. Colloid Interface Sci.* **2025**, *684*, 11−20.
(44) Zhai, M.; Ma, C.; An, J.; Cai, W.; Zhou, T.; Niu, H.; Wang, W. Planar or not planar is A problem. Electrochromic polyamides with the monomer containing dibenzofluorene fused to triphenylamine for smart windows with high contrast ratio aimed for energy conservation. *Eur. Poly. J.* **2025**, *235*, 114074.
(45) Yamazaki, N.; Higashi, F.; Kawabata, J. Studies on reactions of the N-phosphonium salts of pyridines. XI. Preparation of polypeptides and polyamides by means of triaryl phosphites in pyridine. *J. Polym. Sci., Polym. Chem.* **1974**, *12* (9), 2149−2154.
(46) Yamazaki, N.; Matsumoto, M.; Higashi, F. Studies on reactions of the N-phosphonium salts of pyridines. XIV. Wholly aromatic polyamides by the direct polycondensation reaction by using phosphites in the presence of metal salts. *J. Polym. Sci., Polym. Chem.* **1975**, *13* (6), 1373−1380.
(47) Yen, H. J.; Guo, S. M.; Liou, G. S. Synthesis and unexpected electrochemical behavior of the triphenylamine-based aramids with ortho-and para-trimethyl-protective substituents. *J. Polym. Sci., Part A: Polym. Chem.* **2010**, *48* (23), 5271−5281.
(48) Irvin, J. A.; Reynolds, J. R. Low-oxidation-potential conducting polymers: alternating substituted para-phenylene and 3, 4-ethylenedioxythiophene repeat units. *Polymer* **1998**, *39* (11), 2339−2347.
(49) Nhon, L.; Tennyson, S. L.; Butt, M. W.; Bacsa, J.; Tomlinson, A. L.; Reynolds, J. R. Theory-Driven Spectral Control of Bis-EDOT Arylene Radical Cation Chromophores. *Chem. Mater.* **2022**, *34* (21), 9546−9557.
(50) Huang, L. T.; Yen, H. J.; Chang, C. W.; Liou, G. S. Red, green, and blue electrochromism in ambipolar poly (amine−amide−imide)s based on electroactive tetraphenyl-p-phenylenediamine units. *J. Poly. Sci. Part A: Polym. Chem.* **2010**, *48* (21), 4747−4757.

https://doi.org/10.1021/acsapm.5c01973
ACS Appl. Polym. Mater. 2025, 7, 10730−10740